Electronic Supplementary Material (ESI) for Nanoscale.

Length-dependent dual-mechanisms controlled failure modes in silver penta-twinned nanowires

Tianshou Liang[1], Dejian Zhou[1,2,*], Zhaohua Wu[2], Pengpeng Shi[3] and Xiaoyong Chen[2]

[1] School of Mechano-Electronic Engineering, Xidian University, Xi'an 710071, Shaanxi, PR China

[2] School of Mechano-Electronic Engineering, Guilin University of Electronic Technology, Guilin 541004, Guangxi, PR China

[3] A State Key Laboratory for Strength and Vibration of Mechanical Structures, Shaanxi Engineering Research Center of NDT and Structural Integrity Evaluation, School of Aerospace, Xi'an Jiaotong University, Xi'an 710049, Shaanxi, PR China

* Corresponding Author: E-mail: emezdj@guet.edu.cn

SI-1: Evaluation for EAM potentials

The generalized stacking fault energy curve (GSFE), rather than stacking fault energy only, involving both stable and unstable stacking fault energies was found to be adequate to elucidate distinct deformation mechanisms in nanocrystalline metals[1]. In particular, The first energy maximum encountered along the <112> direction is the unstable stacking fault energy (USFE), which represents the lowest energy barrier for dislocation nucleation[2]; the first energy minimum at $a_0/\sqrt{6}$ corresponds to the intrinsic stacking fault energy (ISFE), where a full dislocation dissociates into a pair of Shockley partials[3].

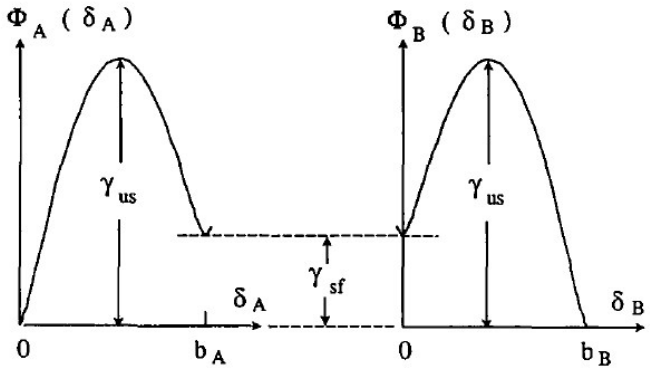

Fig. S1 Energy vs slip for two partial dislocations combined to form a complete lattice dislocation[2].

It was demonstrated that the ratio of stable stacking fault and unstable stacking fault, γ_{sf}/γ_{usf} , was an important parameter for evaluating the deformation mechanism in nanocrystalline[1]. Furthermore, other factors, such as grain size and orientation, were suggested to be taken into account in conjunction with the GSFE for describing the deformation behavior[4], where they suggested that the parameter $\gamma_d \equiv \gamma_{sf}/(\gamma_{usf} - \gamma_{sf})$ was a prime factor used to characterize materials for plastic deformation.

Thus, before exploring the mechanical deformation behavior of nanowires using MD, it is necessary to evaluate the semi-empirical potential function used in MD for capturing the real plastic deformation behavior of nanowires. GSFE curves of several EAM potentials[5-7] were abstained by performed MD calculations following the strategy from references[8]. Then, we compared the results with that of DFT

calculation[9]. Shown as in Fig. S1.

Fig. S2 shows that the unstable stacking fault energy of all MD calculations are all comparable with the DFT calculation, while the intrinsic stacking fault energy of MD calculations show distinct differences and only the results with P. L. wiiliams are comparable with the DFT calculation.

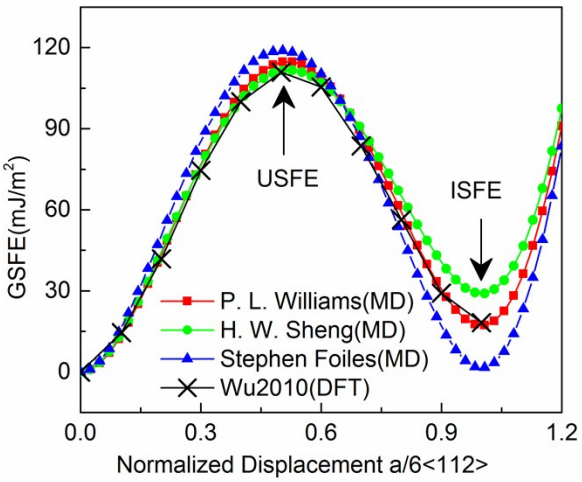

Fig. S2 Generalized stacking fault energy (GSFE) curves for Ag calculated by molecular dynamics (MD) with several semi-empirical potentials and density functional theory (DFT). The peak of the cures indicate the unstable SFE and the minima present intrinsic SFE in plane {111} along <112> direction.

SI-2: Stress deviation at first yield event

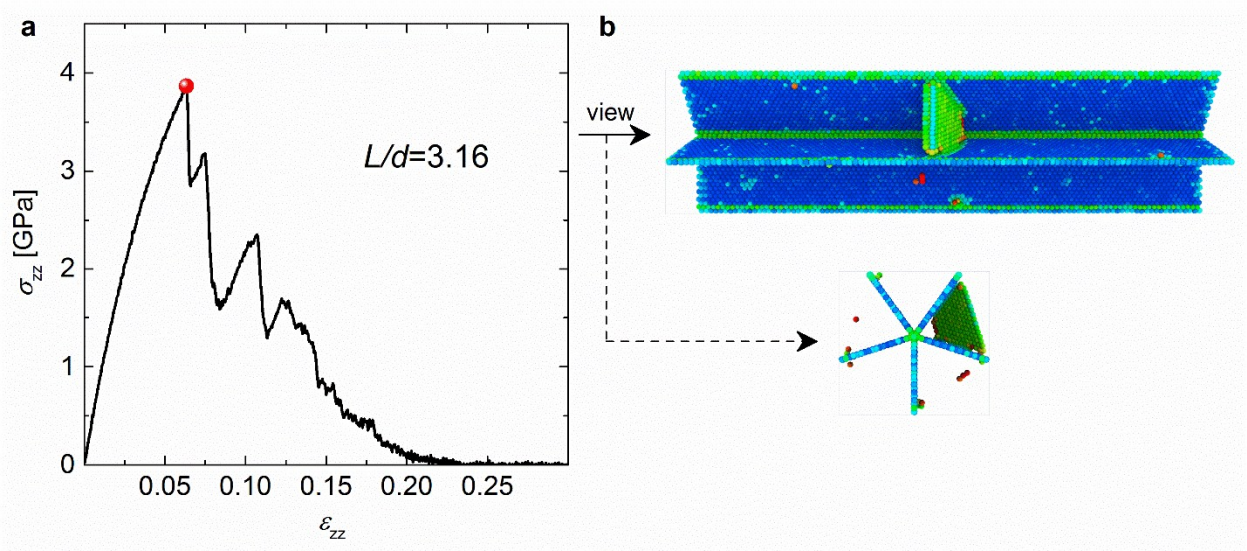

Fig. S3 (a) Stress drop abruptly as it just cross the maximum; (b) nucleation of the first partial dislocation at free surface. The stress drop is attributed to the nucleation of dislocations. *L*/*d*=3.16 represents the aspect ratio (length to diameter) of silver penta-twinned nanowires.

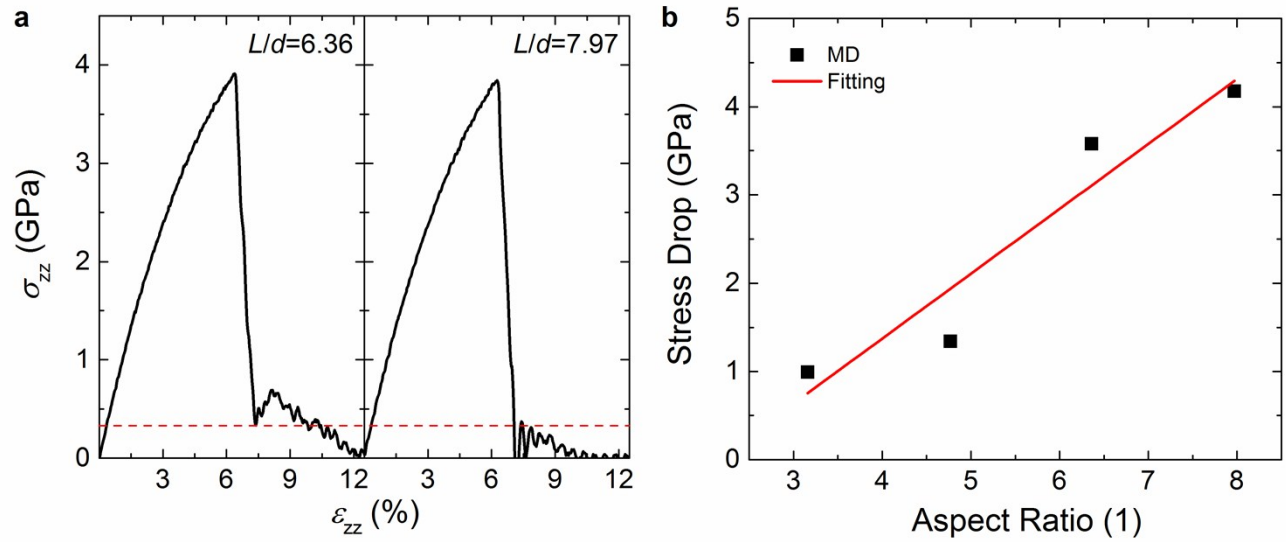

Fig. S4. (a) Uniaxial tensile stress−strain curves of penta-twinned silver nanowires with aspect ratios of 6.36 and 7.97, respectively. (b) Magnitudes of first dorp of flow stress varing with aspect ratios. At point of yield stress, flow stress drop abruptly, the magnitudes of which appear to correlate linearly with the length of nanowires, which corresponds to the behaviours of disloction nucleation at the first stage of plastic deformation. For the nanowires with aspect ratios greater than 6.36, the first drop of flow stress reach bottom of coordinate axis, which could be considered as an indicator for the subsequent plastic deformation exhibits the property of instablity, thus necking arise. See also in Fig. s3

SI-3: Elastic modulus and yield strength

The elastic modulus calculated by fitting the data within the range 0-2% of stress-stain curves at initial elastic deformation are shown in Tab. s1, together with the yield strength achieved when the first partial dislocation event is activated from free surface (see also Fig s1), i.e. the maximum stress value of nanowires.

Tab. S1 The geometric parameters of nanowires with the same width about 10 nm.

Number	aspect ratio (L/d)	Apparent modulus（GPa）	Yield strength（GPa）
1	3.16	84.184	3.865
2	4.77	85.388	3.879
3	6.36	85.545	3.913
4	7.97	84.229	3.844
5	9.56	85.442	3.791
6	11.16	85.260	3.811
7	12.75	84.477	3.799
8	14.35	85.129	3.790
9	15.95	85.126	3.633
10	17.03	84.315	3.645
Average		84.91±0.54	3.80±0.09

SI-4: Aspect-ratio-dependent failure modes

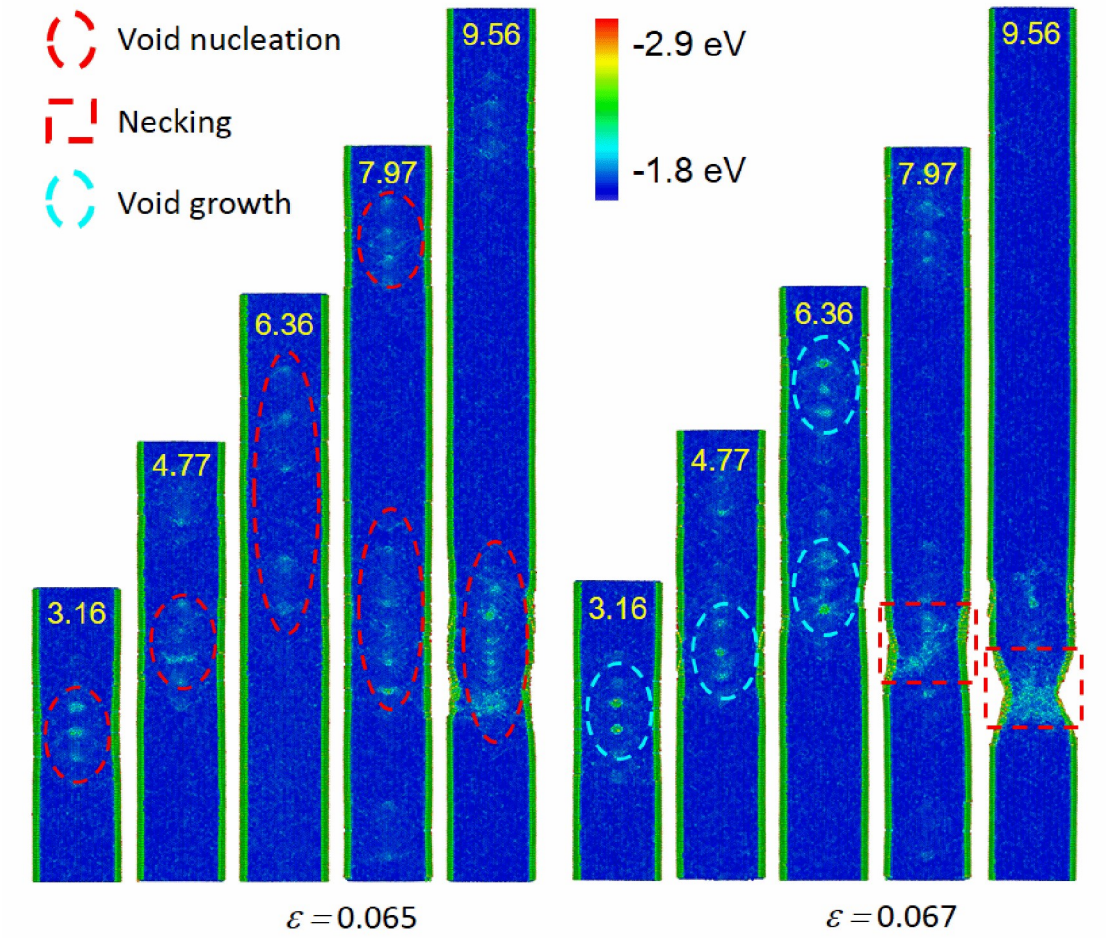

Fig. S5 Snapshots of atomic potential energy of penta-twined Ag nanowires with various aspect ratios (3.16 - 9.56) at initail stage of plastic deformation with strains of ε=0.065 and 0.067. when all nanowires are stretched under strain ε=0.065, the nucleation of pores are observed at some regions along axis, where are marked using red dotted line ellipse. However, when the strain increase to 0.067, the grouth of the pores are only carried out in the nanowires with aspect ratios of 3.16 to 6.36 maked using cyan dotted line ellipse, while for the nanowires with aspect ratios of 7.97 and 9.56, a significant necking behaviour around deformed regions are occurred, where are marked with red dotted line rectangle.

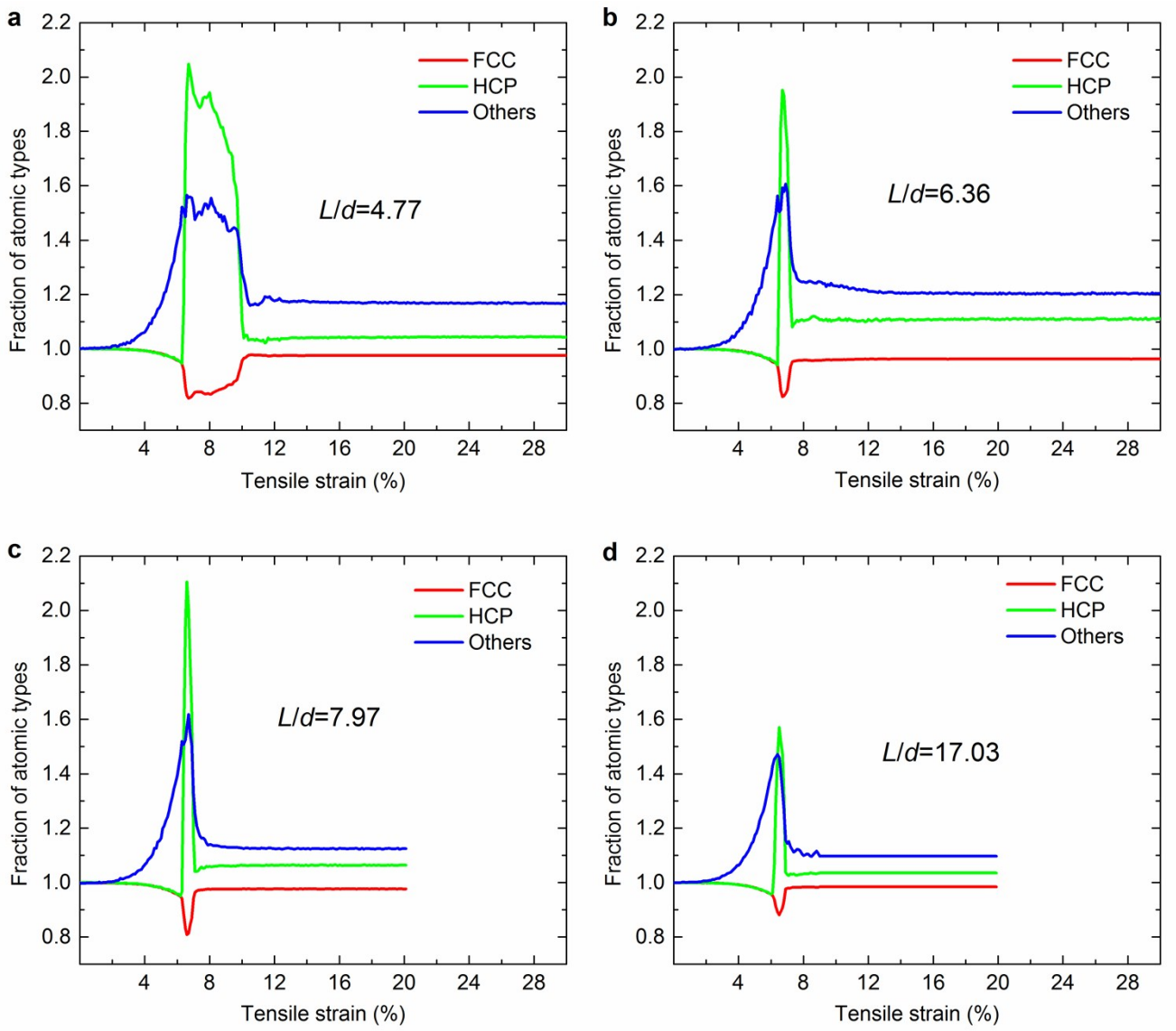

Fig. S6 Variation of the normalized atomic numbers of FCC (red line), HCP (green line), and other atoms including disordering atoms (green line) as function of strain for penta-twined silver nanowires with four aspect ratio. The number of each kind of atoms is normalized by their respective atoms number at strain 0%. Increasing number of HCP atoms indicates the nucleation of partial dislocation, while the decreasing number of HCP atoms corresponds to dislocation recovery or atomic structure disordering.

SI-5: Details of dislocation nucleation

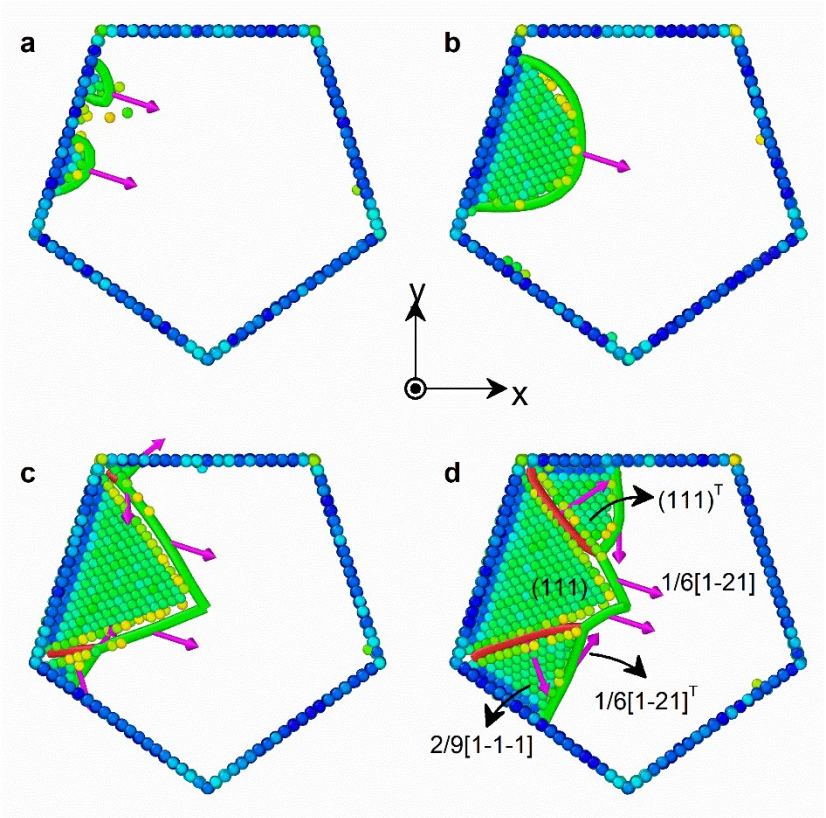

Fig. S7 dislocation nucleation at free surface of silver penta-twinned nanowire. (a) dislocation nucleating; (b) emitting to axis of nanowire; (c) twin boundaries impeding the motion of dislocation; (d) emitting into the adjacent crystals. Shockely partials dislocations with Burgers vector 1/6<112>, partial dislocations with Burgers vector 2/9<111> at the intersection between SFDs and inherent twin boundaries.

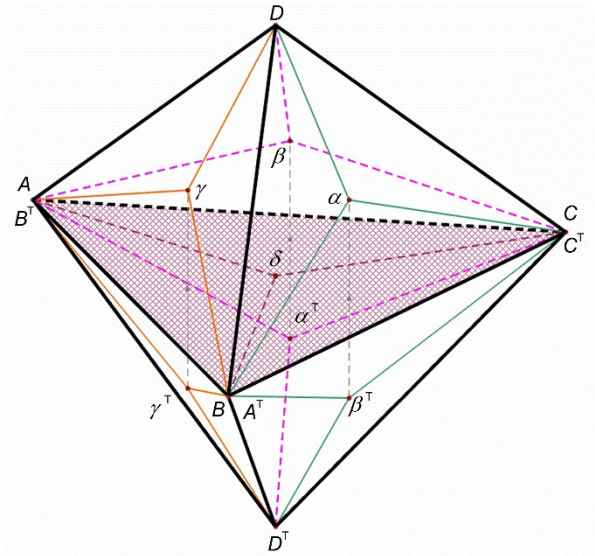

Fig. S8 Illustration of a double Thompson tetrahedron.

Interactions between dislocation and twin boundary:

$\gamma A \rightarrow \gamma' A + \gamma\gamma'$

$\frac{1}{6}[1-21]_{(111)} \rightarrow \frac{1}{6}[1-21]_{(111)_T}^{T} + \frac{2}{9}[1-1-1]$

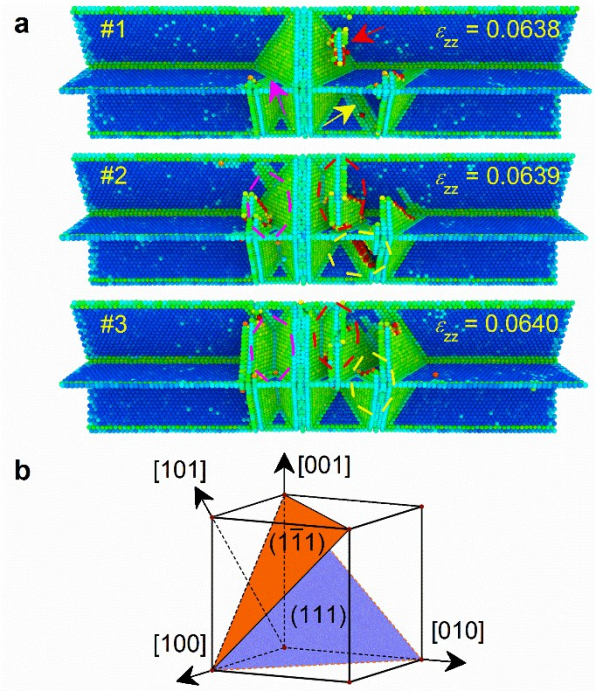

Fig. S9 (a) Atomic configurations of dislocation nucleation, grouth and interaction between dislocations and grain boundaries, and between different dislocations of petten-twined Ag nanowire with aspect ratio of 3.16, which is stretched uniaxially with strains of 0.0638, 0.0639, and 0.064 respectively; (b) schematic diagram of metal fcc unit cell with two equivalent slip systems [101]{111}(colored triangles with light blue and orange). The colored symbols denote the dislocation activities: red for dislocation nucleation (arrow) and grorth (ellipse); yellow for interaction between dislocations and grain boundaries; magenta for interaction between different dislocations.

Fig. s7(a) shows several main behaviors of initial dislocations generated just after yield in penta-twined silver nanowire, including nucleation, propagation and interaction with inherent twin boundaries. Usually, the nucleation of dislocation is activated in free surface of nanowire, i.e. {100}, where is marked using red arrow shown as in Fig. s7(a-#1). Providing a little amount of tension, the propagation of dislocations into the axis of nanowire along two kinds of equilibrium slip planes of {111} shown as in

Fig. s7(b) are captured when ε=0.0639 or 0.064, which are indicated using signs of red dashed ellipse, shown as in Fig. s7 (b-#2 and #3). Furthermore, these two resulted partial dislocations are impeded from each other due to the blocking effect of mutual intersecting. The blocking effect is also carried out in the region marked using magenta signs. In addition to this kind of impediment, the inherent twin boundary is also a key importance role to impede dislocation motion. Once dislocation pierce through the twin boundary, a mirror dislocation is formed in adjacent wedge-shaped crystal, and leaving behind a fixed line defect in the intersection position of dislocation and twin boundary, which are marked with yellow signs. With the number of stacking faults increasing, the stacking fault decahedrons is formed along the axis of nanowires. Hence, the formation of stacking faults and stacking fault decahedrons are responsible for the initial stress drop in nanowires.

The generation and annihilates of dislocations[10]:

1/6[1] → 1/6[1]^{T} + 2/9[] (leading partial Shockley →leading partial Shockley + Frank partial)

2/9[] →1/6[12] + 1/6[12]^{T} (Frank partial → trailing partial Shockley + trailing partial Shockley)

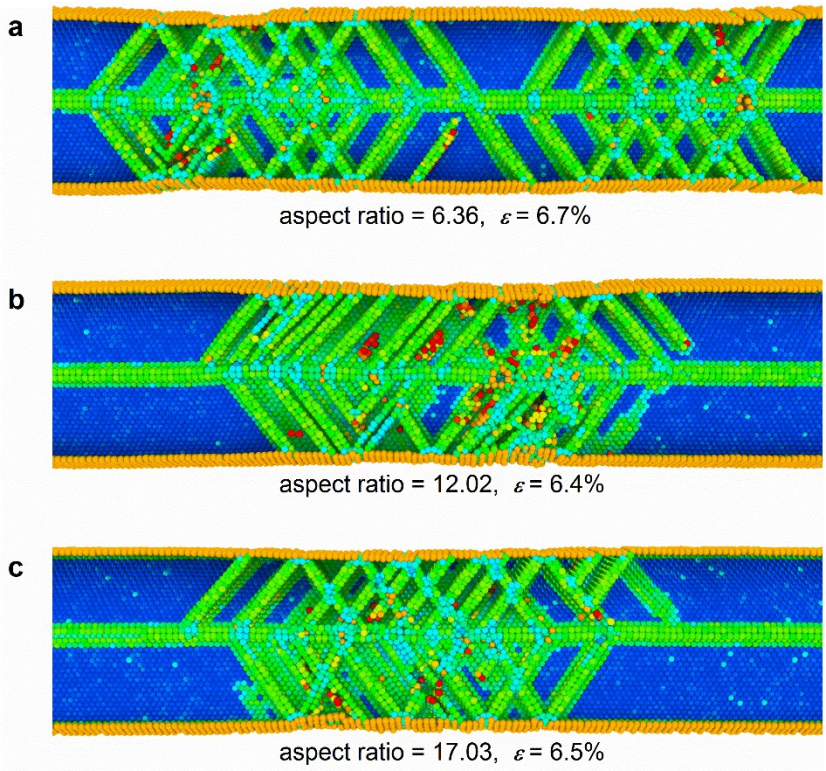

Fig. S10 Patterns of dislocations distributions in penta-twinned Ag nanowires with aspect ratios of 6.36, 12.02, and 17.03 suffered from tensile strains of 6.7%, 6.4%, and 6.5%, respectively. It is shown that the stacking fault decahedrons are the main carrier for producing yield during initial plastic deformation of nanowire with aspect ratio of 6.36 ,while the initial plastic deformation of nanowires with aspect ratios of 12.02 and 17.03 is carried out by a large number of Fan-shaped five-face-structures with same direction. The dislocation density for Fan-shaped five-face-structures is lager that that induced by stacking fault decahedron.

SI-6: Pore-assisted plasticity

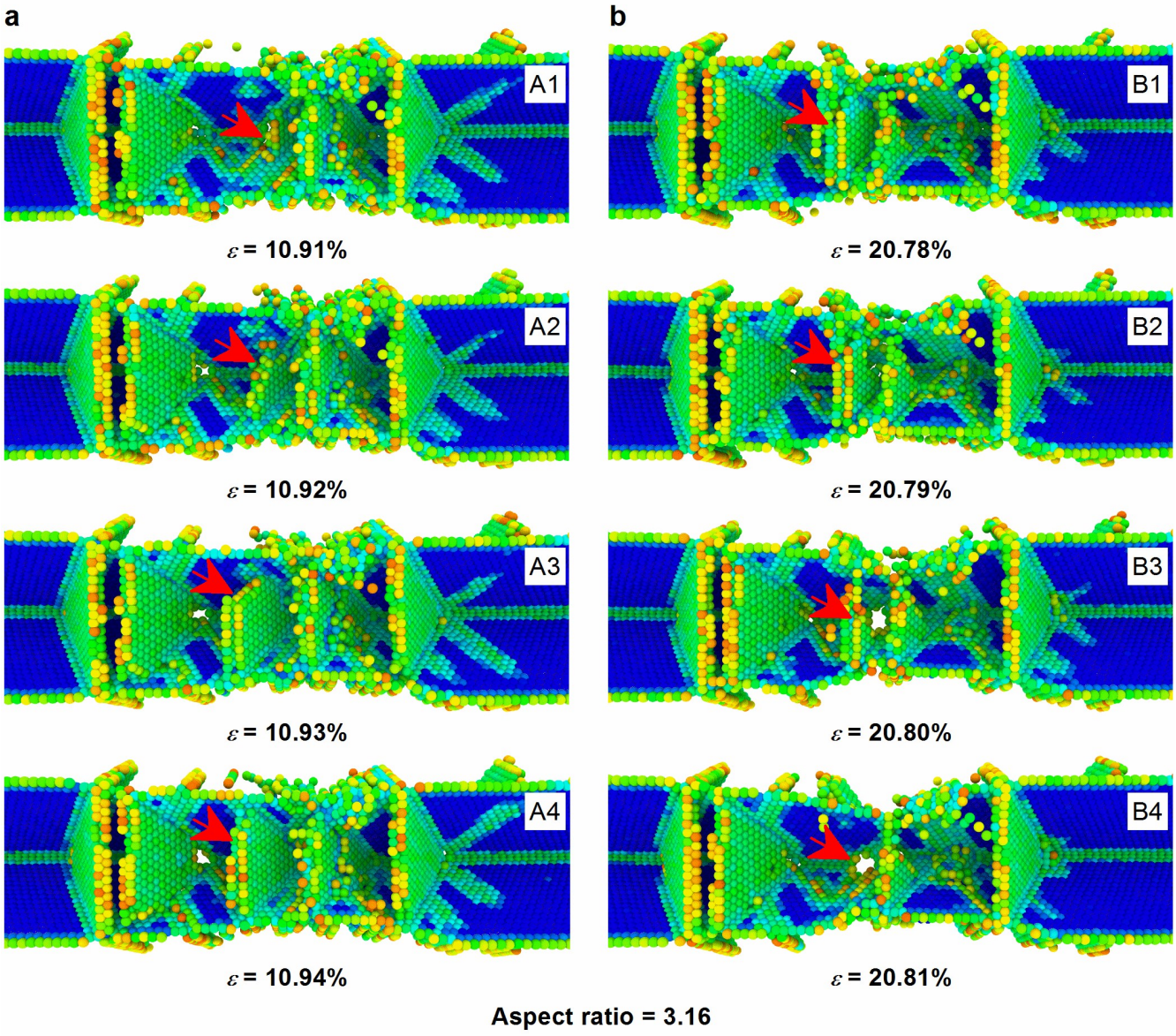

Fig. S11 Pore-assisted plasticity with dislocation motion. The pore, serving as the source of dislocations, emits leading partial dislocation (a) and trailing partial dislocation (b) during the second stage of plastic deformation in short nanowires.

SI-7: Intrinsic stress field and its change characteristics

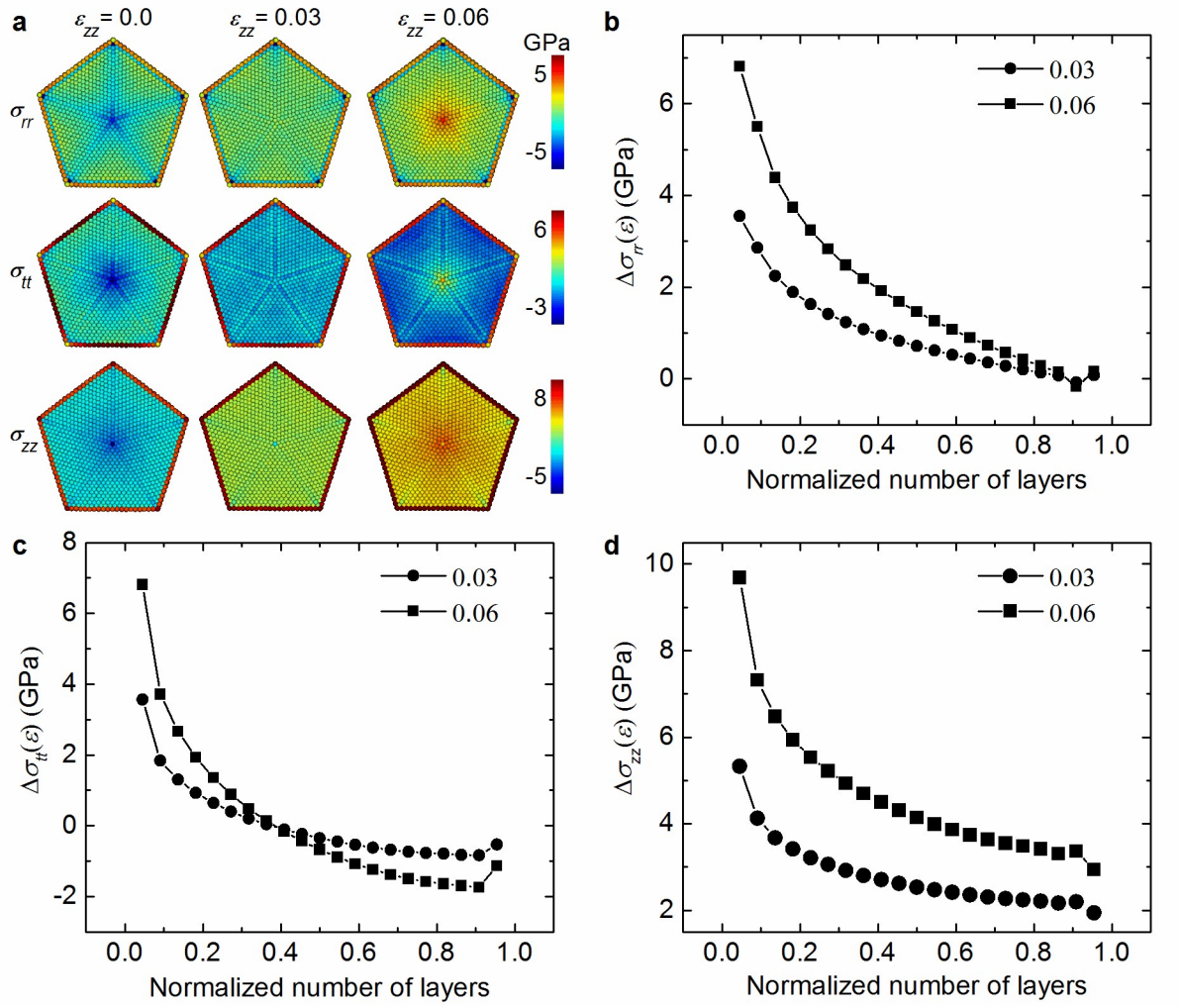

Fig. S12. (a) Stress fields of cross section of naowire with strains of 0.0, 0.03 and 0.06: atomic stress in radial direction σ_{rr} (the first line), tangential direction σ_{tt} (the second line) and along the wire axis σ_{zz} (the last line). For all case, the atomic stress around axial region is compressive stress at the relaxation state, and a transiton of compressive stress to tensile stress is carried out with a strain of about 0.03. (b)-(d) Axial stress increment relatived to initial stress along normalized layer from center to outerlayer with axial strains of 0.03 and 0.06. Quantitatively, the statistical curves about stress increment in radial direction for each atomic layer are shown in figure 6(b-d). For example, figure 6(b) and (c) show that stress components of σ_{rr} and σ_{zz} exhibit a positive increasing trend with increase of tensile strain, and a noteworthy scene is that the increment of stress around surface of nanowire is almost zero for the case of σ_{rr}. Interestingly, figure 6(c) show that these two curves intersect each other at normalized number of about 0.386, which imply that there exit a axial neutral surface where the tangential stress does not change with the increase of tensile loading. Thus contrary to a negative enhancement in σ_{tt} in outer of this neutral surface, the inner region exhibit a positive enhancement. In conclusion, the largest change in stress along axis of nanowire with sign exchanging from compressive stress into tensile stress is confirmed.

SI-8: Dislocation nucleation governed incipient plasticity

As above mentioned, tension stress drops abruptly just when the first dislocation nucleation event arises on the free surfaces of nanowires, which is influenced remarkably by thermal fluctuation and thus is an thermal activation process[11]. The activation parameters such as activation energy and activation volume are usually employed to characterize the activation event. Based on transition state theory[12] (TST), the rate of dislocation nucleation, ν, as a function of pre-tensile stress σ and temperature T, can be expressed as

$$\nu(\sigma,T) = N\nu_0 exp\left[-\frac{Q(\sigma,T)}{k_B T}\right] \qquad (1)$$

where ν_0 is the attempt frequency, k_B is the Boltzmann constant, T is absolute temperature (K), $Q(\sigma,T)$ is activation free energy as function of pre-tensile stress σ and temperature T, and N is the number of equivalent nucleating sites. Here, we applied the approach shown in the works of refs[11, 13] to formulate the activation energy

$$Q(\sigma,T) = Q_0\left(1-\frac{T}{T_{sm}}\right)\left(1-\frac{\sigma}{\sigma_{ath}}\right)^{\alpha} \qquad (2)$$

where σ_{ath} is the athermal strength, T_{sm} is surface atoms disordering temperature, and Q_0 is the energy barrier at zero-T and zero-stress, α is stress sensitivity coefficient. Given equation (2), the activation volume is calculated by the partial derivative of the $Q(\sigma,T)$ with respect to stress σ, i.e. $\Omega(\sigma,T) = -\partial Q(\sigma,T)/\partial\sigma$, which measures the sensitivity of dislocation nucleation rate to stress. Usually, the activation energy of dislocation nucleation for nanowires is calculated using the free-end nudged elastic band (FENEB) method[11, 14]. As shown in Fig. S13a, the energy barrier of a partial dislocation nucleating at free surface of one of wedge-shaped single crystals of silver PTNWs is 0.59 eV under tensile strain 0.052, and several snapshots that depicts dislocation emission process correspond to the curve in Fig. S13a are shown in Fig. S13b. Given the activation parameters, the most probable stress for dislocation nucleation under thermal fluctuation can be predicted by solving the following implicit function equation[11]

$$\frac{Q(\sigma,T)}{k_B T} = ln\left[\frac{k_B T N\nu_0}{E\dot{\varepsilon}\Omega(\sigma,T)}\right] \qquad (3)$$

where E is the apparent Young's modulus, $\dot{\varepsilon} = 10^8$/s is strain rate. For a set of silver PTNWs with constant diameter, the equivalent nucleating sites are correlated with length by N=2*5L/δ, where δ denotes the magnitude of repeat vector a_0<110>/2 (lattice constant a_0=4.09 Å for silver), and the Arabic numerals "2" and "5" account for the two equivalent nucleation systems of <101>{111} at one point in the five wedge-shaped single crystal surface along axial direction.

In order to elucidate the yield events due to dislocation nucleation, we calculated two sets of activation parameters to evaluate the nucleation capacities with respect to average stress over cross section and average stress confined to the atoms close to surface (five layers of atoms), respectively, i.e. total appear activation parameter (TAAP) and local appear activation parameter (LAAP). The former is a common case used in the studies of single crystal or double crystal nanowires[15, 11], while the latter is close to the right parameters that evaluate the true nucleation process due to the anisotropy stress field of cross section of PTNWs.

Given the activation energies Q_0 under different strain calculated by FENEB at 0 K and the average tensile stresses in different regions as mentioned above, shown in Fig. S13c with circular and square solid points, we employed equation (2) to fit the corresponding parameters with T = 0, and get Q_0^{TP}=15.14eV, σ_{ath}^{TP}=7.13GPa, and α^{TP}=4.59 for TAAP, and Q_0^{LP}=25.41eV, σ_{ath}^{LP}=6.37GPa, and α^{LP}=3.52 for LAAP. Moreover, the fitted curves of energy barriers with respect to stress are shown in Fig. S13c, and the corresponding curves of activation volumes are shown in Fig. S13d. Intuitively, the activation parameters of LAAP (blue curves in Fig. S13c and Fig. S13d) are greater than that of TAAP (red curves in Fig. S13c and Fig. S13d) at same level of stress. Specially, when the stress is limited to the range of 3.25 to 4.0 GPa, the LAAP are 2.05 to 0.78eV and 15.38 to 7.68b^3 for energy barrier and activation volume, respectively, while the TAAPs are 0.93 to 0.35eV and 7.28 to 3.37b^3 for energy barrier and activation volume, respectively.

In addition, we solve numerically the equation (3) for the most probable nucleation stress by substituting

ν_0=6.62*10^{11}/s (obtained by calculating the curvature of the minimum energy pathway suggested by Zhu et al.[11]), T=300 K, and T_{sm}=617 K (assumed to be half of the melting point of silver at room temperature), and obtain 3.88 and 3.71 GPa for silver PTNW with length of 15.1 and 161.3 nm, respectively. The theoretical prediction results are similar to that calculated by MD simulation.

It is well known that the smaller the activation parameter is, the more likely the dislocation nucleation occurs. Hence, the result indicates that the ability of nucleating dislocation evaluated by TAAP, closing to the experimental evaluation value, is overestimated relative to that evaluated by LAAPs, similar to the true situation, which is consistent with the implication that the relative low sensitivity of surface stress to tensile strain due to the unique CTBs structure. In comparison, the activation volumes of both cases are close to the results of theoretical predictions (1–10b^3) for Cu single nanowires[11], and the activation volumes in TAAPs are quite close to the fitted values of 1.6–9.2b^3 for silver PTNWs[16]. Whereas the LAAPs are higher than that of the single crystal nanowire or the TAAPs, it is small enough to be susceptible to temperature and strain rate[11] and support the dislocation nucleation serving as the control mechanism in the incipient plasticity of silver PTNWs.

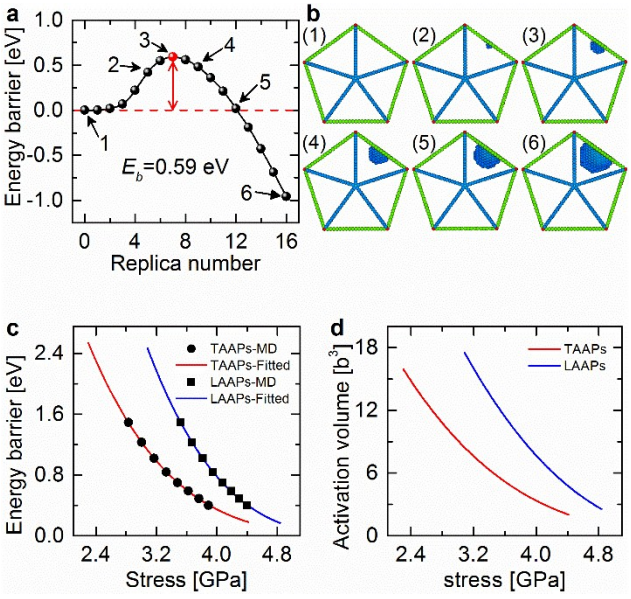

Fig. S13. Activation parameters for dislocation nucleation of silver penta-twinned nanowires. (a) Energy barrier of partial dislocation of silver penta-twinned nanowires with diameter of 10 nm subjected to tensile strain 0.052 at temperature 0 K, calculated using the free-end nudged elastic band method. (b)

Several snapshots of cross section of nanowires showing only stacking fault atoms and surface atoms, describing the evolution of the first dislocation nucleation. (c) Energy barriers as function of average cross-sectional stress (circle solid point and fitted red line) and average surface stress (square solid points and fitted blue line), each value of both corresponding to a shared strain. (d) Activation volumes corresponding to panel (c). The results show that the nucleation capability described by cross section activation parameters (circle solid point and fitted red line) is overestimated due to the anisotropic stress distribution.

Furthermore, recent report[17] shows that the activation parameters of single crystal nanowires highly correlate with diameter varying, because the surface stress of nanowire is sensitive to the variation of diameter in nano scale. Hence, the variation of surface stress of silver PTNWs has significant effect on dislocation nucleation. However, it is beyond the scope of this work, and future work will involve this part of content.

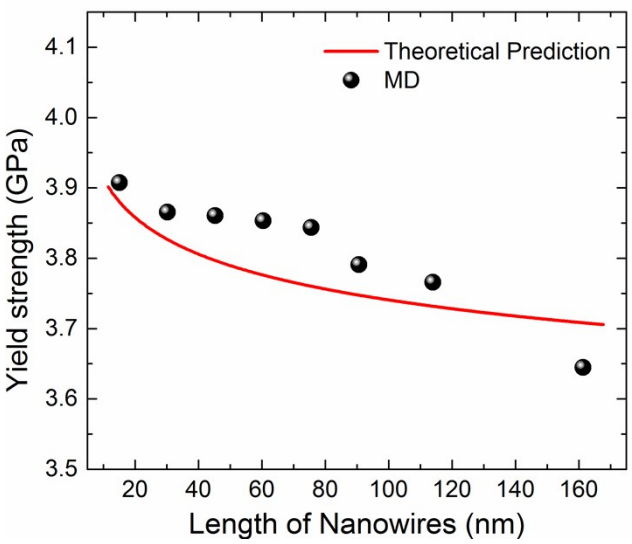

Fig. S14 Yield strength versus the length of nanowires. the small solid balls represent the data calculated by MD simulation, while the red solid curve is abstained by solving numerically the formula (3) suggested by Zhu et al.[11]. The calculated results are consisted with the theoretical prediction values in principle. For more details of the parameters used in this calculation, please refer to the text.

SI-9: Fracture surface morphology and geometric parameters

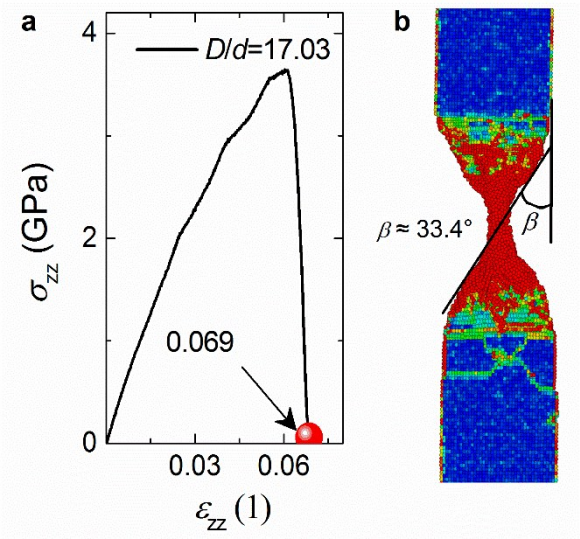

Fig. S15 the morphology of fracture surface when the separation has just happened at stain 0.069. (a) stress-stain curve; (b) fracture surfaces.

SI-10: Calculation of critical aspect ratio of nanowires with shear band

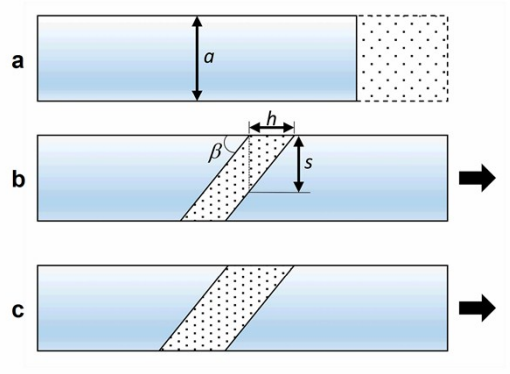

Fig. S16 Diagrammatic sketch of deformation process for silver penta-twined nanowire. (a) Nanowire is at the state of complete relaxation. (b) nanowires is stretched with critical strain, where the first yield event will be activated. (c) Schematic diagram of fracture region structure during yielding process.

In Fig. S13a, the expansion of the volume of nanowires with square cross section, followed what the literatures[18] suggested, due to elastic tension can be calculated by

$$V_c = a^2 L_0 \varepsilon_c$$

The collapse volume of local atoms over the shear region is approximate estimated by

$$V_s = a^2 \cdot h = a^2 \cdot s\cot\beta$$

As described in the text, the difference between volume storing elastic energy and released volume must be positive, which contains the driving energy for slip of shear band, i.e.

$$\Delta V = V_c - V_s \geq 0$$

Hence,

$$L_0 \varepsilon_c \geq s\cot\beta$$

Furthermore, the effective range of shrinkage is $0 \leq s \leq a$. when $s = 0$ indicates a state that shear band has not been activated yet; when $s = a$ signifying two ends of the shear band are about to be separated (Fig. s13c). when s takes the maximum value of a, above inequality all always set up, thus we take $L_0/a \geq \cot\beta/\varepsilon_c$, which is as the same as in the literatures[18, 19].

SI-11: Nanowire stretching process

Mov. s1. showing the evolution of dislocation activities of silver penta-twinned nanowire with L/d=3.16, according which *stable dislocation nucleation mediated incipient plasticity* and then *pore-assisted plasticity with stable dislocation motion* are identified.

Mov. s2. showing the evolution of dislocation activities of silver penta-twinned nanowire with L/d=9.56, according which *unstable dislocation nucleation mediated incipient plasticity* and then *rapid necking* are identified.

References

1 Van Swygenhoven, H., Derlet, P.M. and Froseth, A.G., *Nat. Mater.*, 2004, **3**, 399-403.

2 RICE, J.R., *J. Mech. Phys. Solids*, 1992, **40**, 239-271.

3 Lu, G., Kioussis, N., Bulatov, V.V. and Kaxiras, E., *Phys. Rev. B*, 2000, **62**, 3099-3108.

4 Jo, M., Koo, Y.M., Lee, B., Johansson, B., Vitos, L. and Kwon, S.K., *P. Natl Acad. Sci. Usa*, 2014, **111**, 6560-6565.

5 Williams, P.L., Mishin, Y. and Hamilton, J.C., *Model. Simul. Mater. Sc.*, 2006, **14**, 817-833.

6 Sheng, H.W., Kramer, M.J., Cadien, A., Fujita, T. and Chen, M.W., *Phys. Rev. B*, 2011, **83**.

7 S. M. Foiles, M.I.B.A., *Phys. Rev. B*, 1986, **33**, 7983-7991.

8 Zimmerman, J.A., Gao, H.J. and Abraham, F.F., *Model. Simul. Mater. Sc.*, 2000, **8**, 103-115.

9 Wu, X., Wang, R., Wang, S. and Wei, Q., *Appl. Surf. Sci.*, 2010, **256**, 6345-6349.

10 Wu, Z.X., Zhang, Y.W. and Srolovitz, D.J., *Acta Mater.*, 2009, **57**, 4508-4518.

11 Zhu, T., Li, J., Samanta, A., Leach, A. and Gall, K., *Phys. Rev. Lett.*, 2008, **100**, 25502.

12 Hänggi, P., Talkner, P. and Michal, B., *Rev. Mod. Phys.*, 1990, **62**, 251-341.

13 Ryu, S., Kang, K. and Cai, W., *J. Mater. Res.*, 2011, **26**, 2335-2354.

14 Zhu, T., Li, J., Samanta, A., Kim, H. and Suresh, S., *Proc. Natl. Acad. Sci. U.S.A.*, 2007, **104**, 3031-3036.

15 Ramachandramoorthy, R., Gao, W., Bernal, R. and Espinosa, H., *Nano Lett.*, 2016, **16**, 255-263.

16 Zhang, X., Li, X. and Gao, H., *Acta Mech. Sinica-Prc*, 2017, **33**, 792-800.

17 Li, Q., Xu, B., Hara, S., Li, J. and Ma, E., *Acta Mater.*, 2018, **145**, 19-29.

18 Wu, Z., Zhang, Y., Jhon, M.H., Gao, H. and Srolovitz, D.J., *Nano Lett.*, 2012, **12**, 910-914.

19 Sopu, D., Foroughi, A., Stoica, M. and Eckert, J., *Nano Lett.*, 2016, **16**, 4467-4471.